Numerical analysis of the axial heat conduction with variable fluid properties in a forced laminar flow tube

Lijing Zhai[a], Guoqiang Xu[a], Yongkai Quan[a,*], Gu Song[a],

Bensi Dong[a], Hongwei Wu[b,**]

[a]National Key Laboratory of Science and Technology on Aero-Engine Aero-thermodynamics, School of Energy and Power Engineering, Beihang University, Beijing 100191, China

[b]School of Engineering and Technology, University of Hertfordshire, Hatfield, AL10 9AB, United Kingdom

[*] Corresponding author. Email: quanyongkai@buaa.edu.cn Tel. +86(010)82338335

[**] Corresponding author. Email: h.wu6@herts.ac.uk Tel. +44(0) 1707 284265;

Fax. +44(0) 1707 285086

Abstract

In this article, a theoretical model is developed to investigate the effects of the axial heat conduction on the laminar forced convection in a circular tube with uniform internal heat generation in the solid wall. In the current work, three different fluids, i.e. water, n-decane and air, are selected on purpose since their thermophysical properties show different behavior with temperature. The effects of the axial heat conduction with varying dynamic viscosity and/or varying thermal conductivity are investigated in a systematic manner. Results indicate that the variable-property effects could alleviate the reduction in Nusselt number (*Nu*) due to the axial heat conduction. For the case of Peclet number (*Pe*) equal to 100, wall thickness to inner diameter ratio of 1 and solid wall to fluid thermal conductivity ratio of 100, the maximum *Nu* deviation between constant and variable properties are up to 7.33% at the entrance part for water in the temperature range of 50℃, and 4.45% at the entrance part for n-decane in the temperature range of 120℃, as well as 2.20% at the ending part for air in the temperature range of 475℃, respectively. In addition, the average *Nu* deviation for water, n-decane and air are 3.24%, 1.94% and 1.74%, respectively. Besides, *Nu* decreases drastically with decreasing *Pe* when *Pe*≤500 and with increasing solid wall to fluid thermal conductivity ratio (k_{sf}) when k_{sf} ≤100. It is also found that variable properties have more obvious effects on the velocity profile at the upstream part while more obvious effects on the temperature profile at the downstream part.

Keywords

Conjugate heat transfer; laminar flow; axial heat conduction; variable fluid properties; Nusselt number.

Nomenclature

u_{in}	uniform inlet velocity (m/s)	k_{sf}	solid wall to fluid thermal conductivity ratio
t_{in}	uniform inlet temperature (K)	Nu_z	local Nusselt number
u_m	average axial velocity (m/s)	Re	Reynolds number
u_{max}	maximum axial velocity (m/s)	Pr	Prandtl number
t	temperature (K)	Pe	Peclet number
T	dimensionless temperature	T_f^*	dimensionless fluid bulk temperature
p	pressure (Pa)	T_w^*	dimensionless interfacial wall temperature
P	dimensionless pressure	q^*	dimensionless interfacial heat flux
u	axial velocity (m/s)	$q_{w,in}$	actual interfacial heat flux (W/m^2)
U	dimensionless axial velocity	$q'_{w,in}$	ideal interfacial heat flux (W/m^2)
v	radial velocity (m/s)	z^*	dimensionless axial distance
V	dimensionless radial velocity	ΔNu	Nusselt number deviation (%)
r	radial coordinate (m)		
R	dimensionless radial coordinate	***Greek symbols***	
z	axial coordinate (m)	ρ	density (kg/m^3)
Z	dimensionless axial coordinate	$\dot{\phi}$	internal heat generation (W/m^3)
$u(r)$	axial velocity profile in radial cross-section	δ	wall thickness to inner diameter ratio
$t(r)$	temperature profile in radial cross-section	μ	dynamic viscosity (Pa·s)
L	tube length (m)	Δ	wall thickness (m)
A	cross-sectional area of the tube (m^2)		
m	mass flow rate (kg/s)	***Subscripts***	
r_i	tube inner radius (m)	f	fluid
r_o	tube outer radius (m)	s	solid
d_i	tube inner diameter (m)	w	wall
d_o	tube outer diameter (m)	cp	constant fluid properties
c_p	specific heat capacity (J/kg·K)	vp	variable fluid properties
k	thermal conductivity (W/m·K)	$wall$	considering the axial heat conduction
L_h	theoretical hydrodynamic length (m)		
L_t	theoretical thermal entrance length (m)		

1. Introduction

Conjugate heat transfer problems are not new in concept and have been still extensively studied over the past decades because of its significance in a large variety of engineering applications, such as pipeline petroleum transport, micro-devices as well as aerospace technology. The axial heat conduction has strong effects on heat patterns of the internal flow in channels with thick walls, which are far from the idealized boundary conditions, such as constant outside wall temperature and uniform outside heat flux, on which the available standard heat transfer correlations are based. The discrepancies between experimental results and numerical predictions based on the conventional correlations which neglect the axial heat conduction are frequently reported in scientific literature [1, 2]. Faghri and Sparrow [3] reported that the influence of the axial heat conduction was relatively greater for laminar flow than that for turbulent flow. Their results also showed that the wall axial conduction could easily overwhelm the fluid axial conduction. Therefore, more attention should be paid to the axial heat conduction in the solid region at low Reynolds number [4, 5].

Many analytical, numerical and experimental works have been done in order to reveal the effects of the axial heat conduction on the laminar flow. Zariffeh et al. [6] and Bilir [7] used a finite-difference method to investigate the combined effects of the wall and fluid axial conduction. These studies were based on the assumption of one-dimensional conduction in the solid wall. Quintero and Vera [8] theoretically and numerically studied the multilayered, counterflow, parallel-plate heat exchangers, considering both axial and transverse wall conduction effects. Davis and Gill [9] employed analytical and experimental methods to investigate the Couette flow between parallel plates, studying the parameters that determined the relative importance of the axial wall heat conduction. Adelaja et al. [10] used the separation of

the variables in order to investigate the conjugate heat transfer in tube laminar flow. Axtmann et al. [11] focused on the convective heat transfer in the thermal entrance region of the concentric annuli and proposed Nusselt number correlations of laminar and turbulent internal flows. Furthermore, the axial heat conduction is more prominent in microchannels since the wall thickness is significant compared to the tube's hydraulic diameter, and thus almost all of the microchannels should be considered as a thick-wall type. Detailed research activities were performed in microchannels over the past decades, such as Nonino et al. [12], S. X. Zhang et al. [13], Toh et al. [14] and Gamrat et al. [15].

With respect to the evaluation criteria of the axial heat conduction, Faghri and Sparrow [3], Maranzana et al. [16], Rahimi and Mehryar [17] and Lin et al. [18] defined their own dimensionless wall conduction number *M*, which represented the ratio of the axial heat conduction in the solid wall to the heat convection in the fluid from different angles. Maranzana et al. [16] concluded that the axial conduction could be neglected when *M* was lower than 0.01 for most cases. Lin et al. [18] took the temperature gradient of the solid wall and fluid into consideration to define a modified axial conduction number. According to the conclusions obtained from above studies, whether the effects of the axial heat conduction can be neglected or not is highly situation-dependent and the axial conduction number is not the only criterion.

On the other hand, the assumption of the constant fluid properties is inaccurate, since the fluid flow and heat transfer characteristics in channels with variable fluid properties reveal significant deviations from that with constant properties. Many previous studies paid attention to the influence of the variable properties in macro- or micro-convection within the continuum regime during the last few decades. Kumar and Mahulikar [19] investigated the effects of the temperature-dependent viscosity

variation on the fully developed flow through a microchannel and observed four different flow regions in the flow regime. Ho et al. [20] studied the effects of the temperature-dependent thermophysical properties on the laminar forced convection effectiveness of the Al_2O_3-water nanofluids in a circular tube imposed to a constant heat flux. It was found that the effects of the thermophysical properties on the Nusselt number were more notable with an increase in nanofluid concentration. Ghosh et al. [21] developed a simulation algorithm of the multistream plate fin heat exchangers incorporating the effects of the axial conduction in the heat exchanger core, heat leakage and variable fluid properties. Lelea [22] investigated the conjugate heat transfer of the variable-property water flow inside the microtube and analyzed the influence of the heating position, tube material, wall thickness and *Re* upon the thermal parameters. Nonino et al. [23] investigated the laminar forced convection at the entrance region of the straight ducts with variable viscosity according to an exponential relation by a finite element procedure, considering different cross-sectional geometries. Afterwards, they adopted the same procedure to study the effects of the viscous dissipation and temperature dependent viscosity in thermally and simultaneously developing laminar flows [24]. A series of work by Mahulikar and Herwig were related to the variable-property effects in laminar convection of the incompressible liquid and compressible gas. Mahulikar and Herwig [25] investigated the convection from macro-to-microscale by re-examing the dimensionless governing equations including the dynamic viscosity and thermal conductivity variation. They concluded that the effects of the property variations became highly significant from macro-to-microscale convection, and that the effects of the property variations along the flow became more significant relative to the property variations over the cross section. Similar conclusions were also drawn from their research [26]. Later on, they

made a further analysis of the laminar micro-convection effects due to the variation of the dynamic viscosity and thermal conductivity of the incompressible liquid [27]. After that they paid attention to the laminar micro-convection due to variation of the gas properties [28], incorporating the physical effects of the variation of the gas density with pressure and temperature as well as gas viscosity and thermal conductivity with temperature. Gulhane and Mahulikar [29, 30] explored the forced laminar gas micro-convection due to density, specific heat capacity, viscosity and thermal conductivity variations with entrance effects. Ramiar and Ranjbar [31] studied the effects of the axial conduction and variable properties on two-dimensional conjugate heat transfer of Al_2O_3-EG/water mixture nanofluid in microchannel, concluding that considering variable properties caused higher *Nu* and lower shear stresses compared with constant properties. The main conclusion from these researches is that taking variable-property into consideration is more accurate and more realistic, especially at low *Re* [32, 33].

It appears from the aforementioned investigations that the variable-property effects play a significant role on the fluid flow and heat transfer characteristics. To the best knowledge of the authors, however, the comprehension of the flow and heat transfer mechanism of the axial heat conduction with varying fluid properties has been far from complete and there is still much room to be enhanced in this area. From the mechanism research's point of view, the main objective of the present work is to propose a theoretical model capable of investigating the conjugate heat transfer characteristics with varying fluid properties such as dynamic viscosity and thermal conductivity with an emphasis on the axial heat conduction in a forced laminar flow tube. Therefore, in this work three different fluids, i.e. water, n-decane (C10) and air, are selected in order to achieve a profound comprehension on the heat transfer

mechanism of conjugate heat transfer problems with varying fluid properties.

2. Mathematical model and numerical analysis

2.1. Mathematical model

Fig. 1 illustrates the schematic diagram of the mathematical model. Fluid with uniform velocity u_{in} and temperature t_{in} enters a circular tube with inner radius r_i, wall thickness Δ, and length L. In the current study, the tube length is five times of the thermal entrance length in order to incorporate both developing and fully developed regions. The heat source is associated with a uniform internal heat generation $\dot{\phi}$ applied in the solid wall. The two ends and outside wall of the tube are set as adiabatic conditions. The current work investigates both developing and developed laminar flow, which occurs when velocity and temperature fields develop simultaneously as the heat transfer begins at the duct inlet.

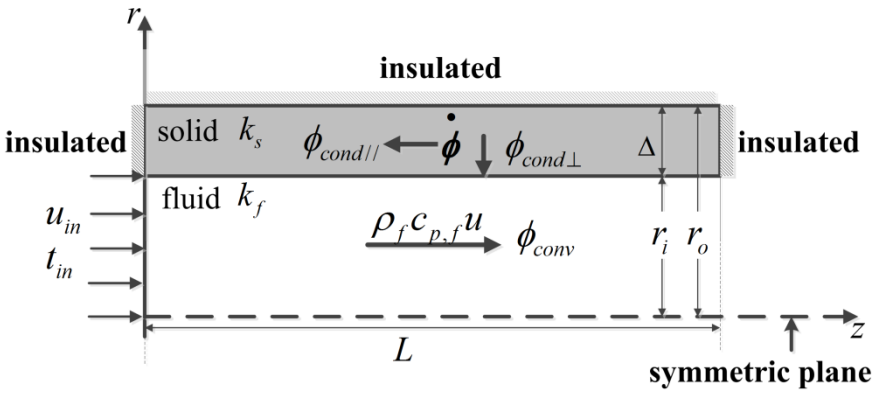

Fig. 1. Schematic diagram of the mathematical model and coordinate system.

The mathematical descriptions are derived from continuum-based equations of mass, momentum and energy. The following major assumptions are employed in the derivations of the governing equations:

(1) Incompressible Newtonian fluid and steady laminar flow.

(2) Thermal conductivity and dynamic viscosity are the only physical properties

varying as a function of temperature while other fluid properties are kept unchanged.

(3) Constant thermal properties of the solid wall.

(4) Negligible effects of electromagnetic forces, gravity and other body forces.

(5) Negligible radiation heat transfer.

(6) Negligible heat generation due to viscous dissipation.

(7) No slip flow and no temperature jump.

Other simplifications are described in due course in the rest of the paper.

Based on the above assumptions, in the present study, two-dimensional steady flow and heat transfer of the incompressible fluids will be taken into account. The continuity equation (1), momentum equations (2) and (3) in axial and radial directions, as well as energy equations (4) and (5) in the fluid and solid regions, respectively, are as follows.

Continuity equation:

$$\frac{\partial\left(\rho_f u\right)}{\partial z}+\frac{1}{r}\frac{\partial\left(\rho_f r v\right)}{\partial r}=0 \tag{1}$$

Momentum equations:

$$\frac{\partial\left(\rho_f u u\right)}{\partial z}+\frac{1}{r}\frac{\partial\left(r\rho_f v u\right)}{\partial r}=-\frac{\partial p}{\partial z}+\frac{\partial}{\partial z}\left(\mu_f\frac{\partial u}{\partial z}\right)+\frac{1}{r}\frac{\partial}{\partial r}\left(r\mu_f\frac{\partial u}{\partial r}\right) \tag{2}$$

$$\frac{\partial\left(\rho_f u v\right)}{\partial z}+\frac{1}{r}\frac{\partial\left(r\rho_f v v\right)}{\partial r}=-\frac{\partial p}{\partial r}+\frac{\partial}{\partial z}\left(\mu_f\frac{\partial v}{\partial z}\right)+\frac{1}{r}\frac{\partial}{\partial r}\left(r\mu_f\frac{\partial v}{\partial r}\right)-\mu_f\frac{v}{r^2} \tag{3}$$

Energy equations:

Liquid $$\frac{\partial\left(\rho_f c_{p,f} u t_f\right)}{\partial z}+\frac{1}{r}\frac{\partial\left(r\rho_f c_{p,f} v t_f\right)}{\partial r}=\frac{\partial}{\partial z}\left(k_f\frac{\partial t_f}{\partial z}\right)+\frac{1}{r}\frac{\partial}{\partial r}\left(rk_f\frac{\partial t_f}{\partial r}\right) \tag{4}$$

Solid $$\frac{\partial}{\partial z}\left(k_s\frac{\partial t_s}{\partial z}\right)+\frac{1}{r}\frac{\partial}{\partial r}\left(rk_s\frac{\partial t_s}{\partial r}\right)+\dot{\phi}=0 \tag{5}$$

where ρ_f, $c_{p,f}$, k_f and μ_f are the fluid density, specific heat capacity, thermal

conductivity and dynamic viscosity, respectively; $\dot{\phi}$ is the internal heat generation in the solid wall, W/m^3.

According to the physical problem described in Fig.1, the boundary conditions can be mathematically summarized as follows:

$$\begin{cases} z=0,\ 0\le r\le r_i,\ u=u_{in},\ v=0,\ t_f=t_{in} \\ z=0,\ r_i\le r\le r_o,\ u=v=0,\ \dfrac{\partial t_s}{\partial z}=0 \\ z=L,\ r_i\le r\le r_o,\ u=v=0,\ \dfrac{\partial t_s}{\partial z}=0 \\ r=0,\ 0\le z\le L,\ \dfrac{\partial u}{\partial r}=0,\ v=0,\ \dfrac{\partial t_f}{\partial r}=0 \\ r=r_i,\ 0\le z\le L,\ u=0,\ v=0,\ t_s=t_f,\ k_f\dfrac{\partial t_f}{\partial r}=k_s\dfrac{\partial t_s}{\partial r} \end{cases} \tag{6}$$

In order to generalize results, the non-dimensional governing equations and boundary conditions are derived in the following:

Continuity equation:

$$\frac{\partial U}{\partial Z}+\frac{1}{R}\frac{\partial(RV)}{\partial R}=0 \tag{7}$$

Momentum equations:

$$\frac{\partial(UU)}{\partial Z}+\frac{1}{R}\frac{\partial(RUV)}{\partial R}=-\frac{\partial P}{\partial Z}+\frac{\partial}{\partial Z}\left(\frac{2}{Re}\frac{\partial U}{\partial Z}\right)+\frac{1}{R}\frac{\partial}{\partial R}\left(R\frac{2}{Re}\frac{\partial U}{\partial R}\right) \tag{8}$$

$$\frac{\partial(UV)}{\partial Z}+\frac{1}{R}\frac{\partial(RVV)}{\partial R}=-\frac{\partial P}{\partial R}+\frac{\partial}{\partial Z}\left(\frac{2}{Re}\frac{\partial V}{\partial Z}\right)+\frac{1}{R}\frac{\partial}{\partial R}\left(R\frac{2}{Re}\frac{\partial V}{\partial R}\right)-\frac{2}{Re}\frac{V}{R^2} \tag{9}$$

Energy equations:

Liquid $$\frac{\partial(UT_f)}{\partial Z}+\frac{1}{R}\frac{\partial(RVT_f)}{\partial R}=\frac{\partial}{\partial Z}\left(\frac{2}{Pe}\frac{\partial T_f}{\partial Z}\right)+\frac{1}{R}\frac{\partial}{\partial R}\left(R\frac{2}{Pe}\frac{\partial T_f}{\partial R}\right) \tag{10}$$

Solid $$\frac{\partial^2 T_s}{\partial Z^2}+\frac{1}{R}\frac{\partial}{\partial R}\left(R\frac{\partial T}{\partial R}\right)+\bar{\dot{\phi}}\frac{1}{k_{sf}}=0 \tag{11}$$

The non-dimensionl parameters in Eqs. (7)-(11) are defined as below:

$$\bar{\dot{\phi}} = \frac{\dot{\phi} \cdot r_i}{q'_{w,in}} = \frac{2r_i^2}{r_o^2 - r_i^2} = \frac{(d_i - 2\Delta)^2}{2\Delta(d_i - \Delta)} = \frac{(1-2\delta)^2}{2\delta(1-\delta)}, Z = \frac{z}{r_i}, R = \frac{r}{r_i}, U = \frac{u}{u_{in}}, V = \frac{v}{u_{in}}, P = \frac{p}{\rho_f u_{in}^2},$$
$$T = \frac{k_f (t - t_{in})}{q'_{w,in} \cdot r_i}, k_{sf} = \frac{k_s}{k_f}, Re = \frac{\rho_f u d_i}{\mu_f}, Pr = \frac{\mu_f c_{p,f}}{k_f}, \quad Pe = Re \times Pr = \frac{u d_i \rho_f c_{p,f}}{k_f}.$$

where k_{sf} stands for solid wall to fluid thermal conductivity ratio, defined as $k_{sf} = k_s / k_f$; δ stands for wall thickness to inner diameter ratio, defined as $\delta = \Delta / d_i$; Δ is the wall thickness.

These equations are solved under the following boundary conditions:

$$\begin{cases} Z = 0,\ 0 \le R \le 1.0,\ U = 1.0,\ V = 0,\ T_f = 0 \\ Z = 0,\ 1.0 \le R \le \dfrac{r_o}{r_i},\ U = V = 0,\ \dfrac{\partial T}{\partial Z} = 0 \\ Z = \dfrac{L}{r_i},\ 1.0 \le R \le \dfrac{r_o}{r_i},\ U = V = 0,\ \dfrac{\partial T_s}{\partial Z} = 0 \\ R = 0,\ 0 \le Z \le \dfrac{L}{r_i},\ \dfrac{\partial U}{\partial R} = 0,\ V = 0,\ \dfrac{\partial T_f}{\partial R} = 0 \\ R = 1.0,\ 0 \le Z \le \dfrac{L}{r_i},\ U = 0,\ V = 0,\ T_s = T_f,\ k_f \dfrac{\partial T_f}{\partial R} = k_s \dfrac{\partial T_s}{\partial R} \end{cases} \tag{12}$$

The dimensionless governing equations above suggest that the axial heat conduction mainly depends on four parameters, such as *Pr*, *Re*, the dimensionless parameter k_{sf} and δ. For a given fluid, axial heat conduction depends on only three parameters: *P*e, k_{sf} and δ since *Pe* equals to the product of *Pr* and *Re*. The local Nusselt number for the circular cross-section tube is defined in Eq. (13).

$$Nu_z = -\frac{d_i \left.\dfrac{\partial t_f}{\partial r}\right|_{r=r_i}}{(t_w - t_f)} = \frac{q_{w,in} d_i}{k_f (t_w - t_f)} \tag{13}$$

where t_f is the fluid bulk temperature, which is the average fluid temperature weighted by the mass flow rate; t_w is the wall temperature at the solid-fluid interface; $q_{w,in}$ is the actual heat flux density with the unit of W/m^3 calculated at the inside

surface of the tube wall which depends on axial distance *z*; $q_{w,in}^{'}$ is the ideal heat flux density calculated according to $\dot{\phi}$ as follows:

$$q_{w,in}^{'} = \frac{\dot{\phi}\left(r_o^2 - r_i^2\right)}{2r_i} \tag{14}$$

In the following sections the dimensionless interfacial heat flux q^*, temperature T^* and *Re* are defined in Eq.(15-17) respectively:

$$q^* = \frac{q_{w,in}}{q_{w,in}^{'}} \tag{15}$$

$$T^* = \frac{\left(t - t_{in}\right)k_f}{q_{w,in}^{'} \cdot r_i} \tag{16}$$

$$Re = \frac{2r_i u_m \rho_f}{\mu_f} \tag{17}$$

where u_m is the average velocity of the fluid, defined as $u_m = m/\left(\rho_f A\right)$.

According to [34], the theoretical hydrodynamic and thermal entrance lengths are given in Eq. (18a) and (18b).

$$L_h = 0.05 d_i Re \tag{18a}$$

$$L_t = 0.05 d_i RePr \tag{18b}$$

2.2. Numerical method and validation

In the current work, the commercially available computational fluid dynamics (CFD) software, ANSYS CFX 15.0, was used to solve the governing equations with imposed boundary conditions mentioned above. A mass-flow-inlet and temperature-inlet were set as the inlet boundary conditions, and a pressure-outlet was set as the outlet boundary condition. The element-based finite volume method (FVM) was used to discretize the governing equations and imposed boundary conditions [35].

The second order high resolution was used for the discretization of the convective term. Furthermore, the SIMPLE algorithm [36] was adopted to deal with the pressure-velocity coupling. The internal wall was set to satisfy no slip and no penetration conditions. Since the governing equations are coupled and thus there was no need to specify the interfacial boundary condition between the fluid and solid domain. The iterations were continued until a converged solution was obtained with root mean square residuals less than 10^{-7} for all the variables.

The laminar flow of water with constant properties in a circular tube without solid region and with uniform heat flux over the entire wall surface was considered as a reference. Under these conditions, the accurate analytical value of *Nu* for fully developed flow is reported 48/11(appropriate 4.364) [37]. The grids in axial direction were uniform while the grids in radial direction were nonuniform with mesh refinement near the inner wall surface shown in Fig. 2.

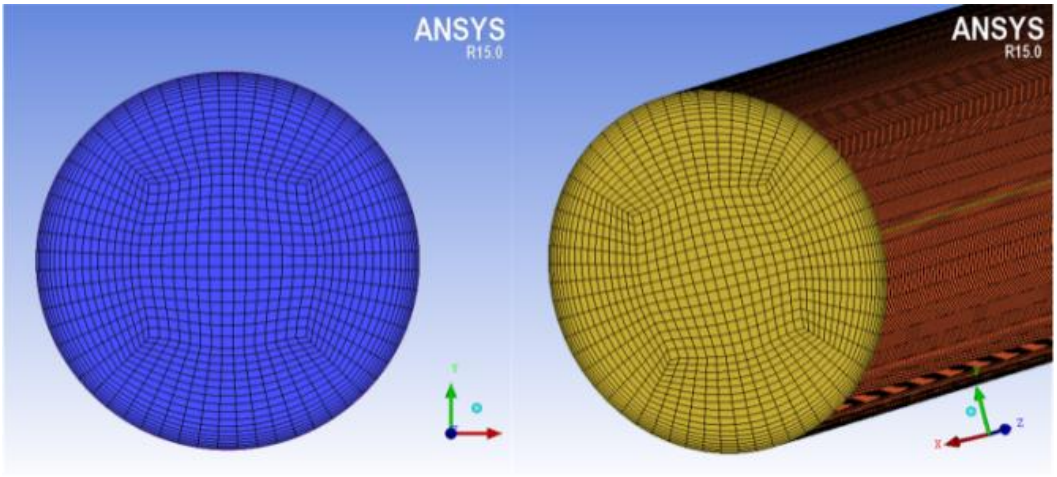

Fig. 2. Computational channel mesh.

The grid independence study was conducted to identify an appropriate grid density for the aimed calculations. The computational domain included both the fluid and solid wall regions, which were discretized using five different grid arrangements of 12×1000, 16×1000, 20×1000, 24×1000 and 28×1000. The numerical results of

the local Nusselt number (Nu_z) versus dimensionless axial distance $z^* = z/(r_i Pe)$ are presented in Fig. 3. Besides, table 1 illustrates the relative differences of Nu_z in the fully developed region between simulated and analytical values for different grid arrangements.

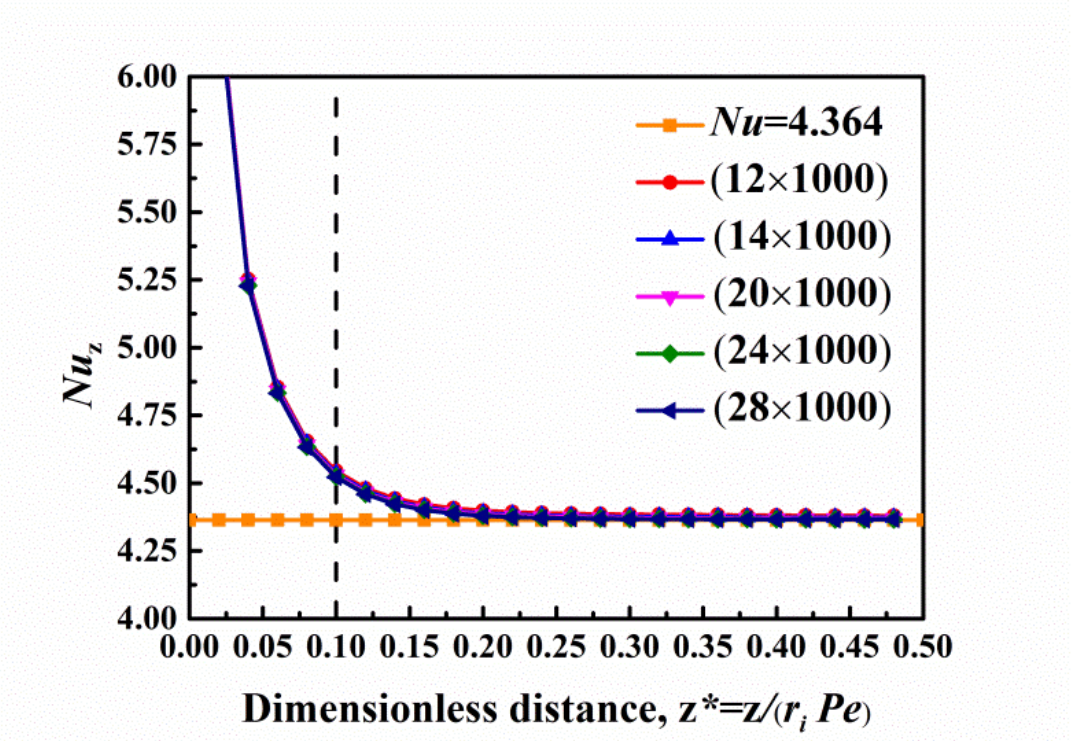

Fig. 3. Grid independent study. (water, *Re*=14.3, *Pr*=7, $\Delta / d_i = 0$)

Table 1 Relative differences between simulated values and analytical values.

Grid arrangement	Simulation error (%)
Radial*Axial	(*Nu*-4.364)/4.364×100
12×1000	0.425
16×1000	0.254
20×1000	0.151
24×1000	0.075
28×1000	0.067

In Fig. 3, it is apparent that the simulated fully developed Nu_z generally agrees with the analytical value with a relative error lower than 0.425% at various grid arrangements. The vertical line of z^*=0.1 stands for the dimensionless thermal entrance length predicted by Eq. (18b), which is only an experimental correlation not

a precise expression, and hence a deviation can be observed. The axial velocity profile and temperature profile in cross-section in fully developed laminar flow have analytical solutions as follows [37].

$$u = 2u_m\left[1-\left(\frac{r}{r_i}\right)^2\right] = u_{\max}\left[1-\left(\frac{r}{r_i}\right)^2\right] \tag{19}$$

$$t - t_w = -\frac{q_w}{k_f r_i}\left(\frac{3}{4}r_i^2 + \frac{r^4}{4r_i^2} - r^2\right) \tag{20}$$

According to the above equations, for grid arrangement of 24×1000, the analytical velocity/temperature profiles and simulated velocity/temperature profiles at z^*=0.25 are shown in Table 2, in which the adjust R-square of simulations is 1.

Table 2 Velocity and temperature profiles of analytical solution and simulated solution.

Velocity/temperature profiles	Analytical solution	Simulated solution
$u(r)$	$-223.783r^2 + 0.00358$	$-223.997r^2 - 1.49351\times10^{-9}r + 0.00358$
$t(r)$	$-2.44145\times10^{10}r^4 + 1.56253\times10^6 r^2 + 310.89$	$-2.42908\times10^{10}r^4 + 9.96208r^3 + 1.5577\times10^6 r^2 + 4.01613\times10^{-4}r + 310.94$

From Table 2, it can be seen that at the grid arrangement of 24×1000, both the temperature and velocity profiles in the fully developed region show good agreements with analytical solutions. Furthermore, as shown in Table 1, from grid arrangement of 24×1000 to 28×1000, the grid number increases by 37.12% while simulation error decreases by just 0.01%. Therefore, the grid arrangement of 24×1000 for the computational domain has satisfactory grid-independence and is sufficient to resolve the conjugate heat transfer problem in forced laminar flow.

3. Results and discussion

3.1. Axial heat conduction with constant fluid properties

For the purpose of comparison, the effects of the axial heat conduction with

constant properties are studied firstly in order to gain a deep understanding of the axial conduction effects with variable fluid properties. As previously stated, for a given fluid, the degree of the axial heat conduction is only determined by *Pe*, k_{sf} and δ. The influence of these parameters on the axial heat conduction will be discussed in detail in this section. In the present study, water with constant properties is chosen as the benchmark case. Four different values of *Pe* i.e., 30, 100, 500 and 1000, together with three different k_{sf} values of 1, 100 and 500, as well as three different values of Δ, namely, $0.5d_i$, $1d_i$ and $2d_i$ are considered. The k_{sf} values representing the thermal conductivity ratio of solid wall to fluid are selected according to [13] in practical applications. Table 3 is a summary of the value arrangements for numerical simulations. A total of 36 simulations are carried out to allow for all the possible combinations. The effects of *Pe*, k_{sf} and δ on the local Nusselt number Nu_z, the dimensionless interfacial heat flux q^*, dimensionless fluid bulk temperature T_f^* and dimensionless interfacial wall temperature T_w^*, are shown in Fig.4, Fig.5 and Fig.6, respectively, with reference to representative cases. There are three straight dot lines in Fig.4a, Fig.5a and Fig.6a. The horizontal lines of Nu=4.364 and Nu=3.66 stand for the analytical values of fully developed *Nu* under constant heat flux boundary condition and constant temperature boundary condition, respectively. The vertical line of z^*=0.1 stands for the thermal entrance length predicted by Eq. (18b).

Table 3 Value arrangements for numerical simulations.

Re	*Pe*	k_s / k_f	Δ / d_i	L / d_i
4.28	30	1	0.5	7.5
14.28	100	100	1	25
71.40	500	500	2	125
142.80	1000			250

3.1.1. Influence of Pe, k_{sf} and δ on q^*, T_f^* and T_w^*

It is recognized that the axial wall heat conduction can result in more heat conduction toward the entrance where temperature of the wall is lower due to the higher convective heat transfer coefficient, as shown in Fig. 4d, Fig. 5d and Fig. 6d. Thus, more heat enters the fluid at the entrance whereas less heat enters the fluid at the exit according to the conservation of the total heat. The effects of the axial heat conduction on q^*, T_f^* and T_w^* can be summarized as follows: (1) axial heat conduction can lead to the fluid bulk temperature increase, deflecting from linear distribution for those without axial heat conduction, as demonstrated in Fig. 4c, Fig. 5c and Fig. 6c; (2) axial heat conduction forces the interfacial wall temperature to increase in the upstream part while to decrease in the downstream part, approaching uniform wall temperature boundary condition, as shown in Fig. 4d, Fig. 5d and Fig. 6d; (3) axial heat conduction can affect the interfacial heat flux higher in the upstream part while lower in the downstream part, departing from uniform heat flux boundary condition, as illustrated in Fig. 4b, Fig. 5b and Fig. 6b; (4) consequently, axial heat conduction lowers Nu_z along the tube relative to those under constant heat flux boundary condition at the solid-fluid interface, as shown in Fig. 4a, Fig. 5a and Fig. 6a.

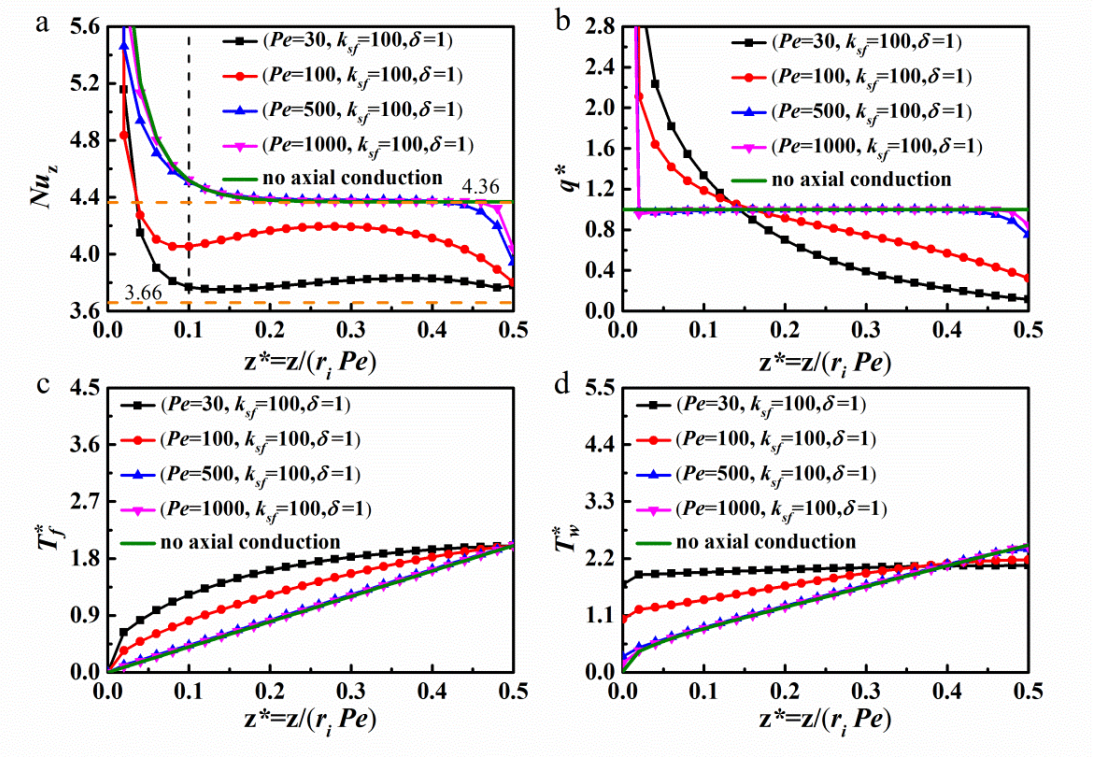

Fig. 4. Effects of *Pe* on the axial distribution of a: Nu_z; b: q^*; c: T_f^*; d: T_w^*.

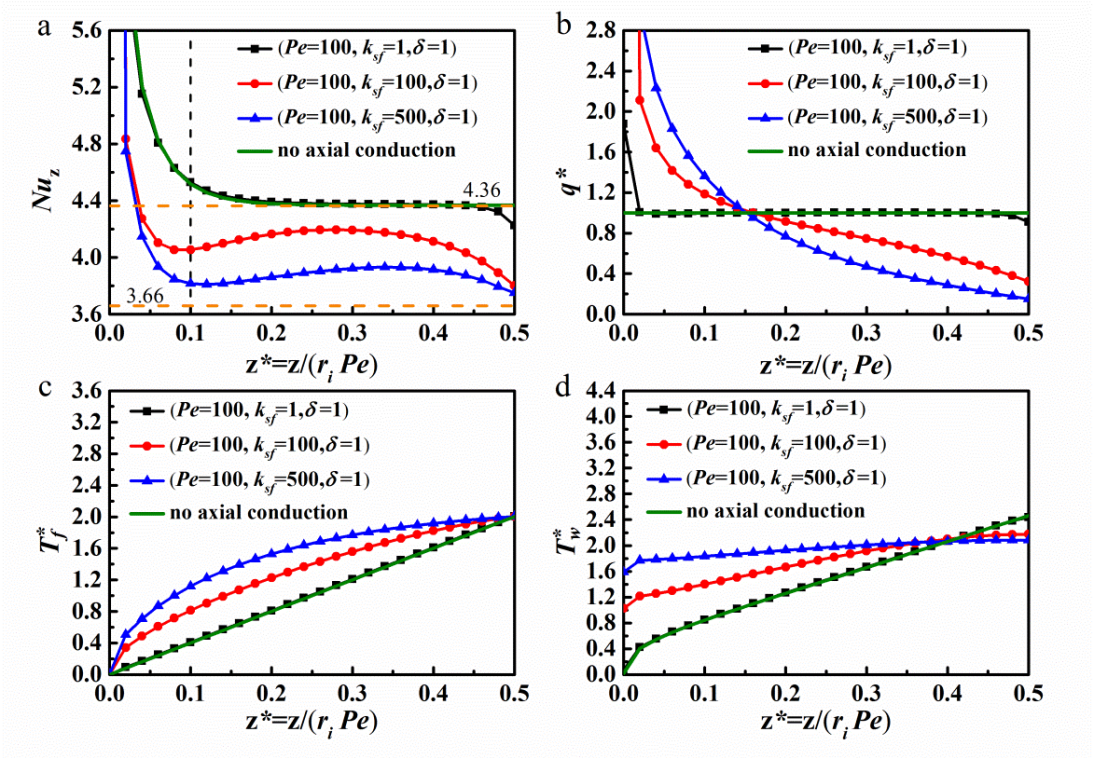

Fig.5. Effects of k_{sf} on the axial distribution of a: Nu_z; b: q^*; c: T_f^*; d: T_w^*.

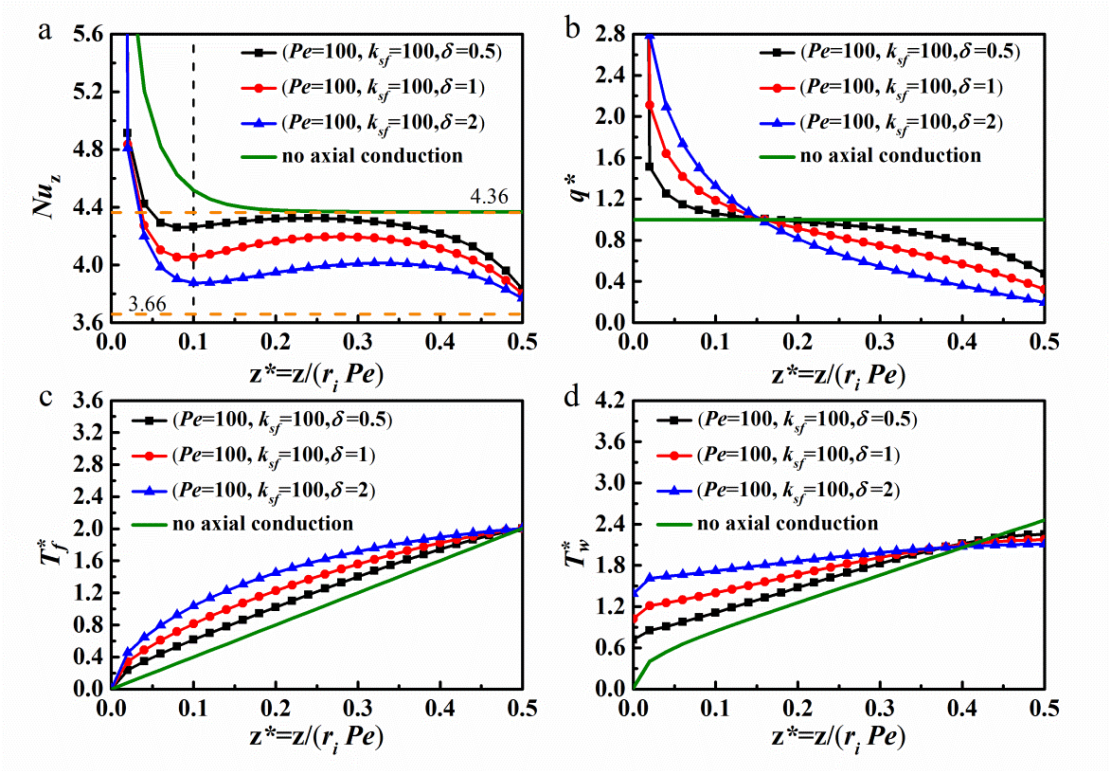

Fig. 6. Effects of δ on the axial distribution of a: Nu_z; b: q^*; c: T_f^*; d: T_w^*.

Fig. 4 shows that the axial heat conduction becomes more dominant with the increase of *Pe*. Increasing *Pe* can decrease the thermal resistance across the flow and further decrease the effects of axial heat conduction. As shown in Fig. 5, the axial heat conduction becomes more significant as k_{sf} increases. Since k_{sf} is the ratio of the thermal resistance in the flow to that in the wall, with increasing k_{sf} axial heat conduction in the wall increases due to the wall thermal resistance reduction. It can be observed from Fig. 6 that the larger δ implies the more significant axial heat conduction. With respect to δ, compared to that in the axial direction, the higher the ratio, the larger the thermal resistance in the radial direction. Thus, it is more likely to conduct more heat to the upstream of the tube. It can be generally observed from above figures that the axial heat conduction becomes more dominant with increasing k_{sf} and δ as well as with decreasing *Pe*.

3.1.2. Effects of the axial heat conduction on Nusselt number

The following noticeable features of *Nu* can be observed from Fig. 4a, Fig. 5a and Fig. 6a:

(1) It is noted that the axial heat conduction has the generalized effects of reducing Nu_z with respect to the "no wall" case. As the effects of the axial heat conduction become more significant, Nu_z in the intermediate part gradually decreases from 4.36 to 3.66. Taking the axial heat conduction into account, the circular tube may experience a boundary condition transformation: from the uniform outside heat flux boundary condition to the constant outside wall temperature boundary condition.

(2) The results show that the axial heat conduction causes Nu_z to decrease sharply at both the entrance and exit of the tube, which can lead to a reduction in average *Nu*. Similar behavior is also found but will not be repeated here. The sharp drop of Nu_z at the entrance can be explained by the fact of the entrance effects [32] while the sharp reduction in Nu_z at the exit can be explained by the influence of the axial heat conduction, which causes more heat enters the fluid at the entrance whereas less heat enters the fluid at the exit on account of the conservation of the total heat. Thus, it appears to be a sharp drop of Nu_z at the exit.

(3) It is recognized that the axial heat conduction causes Nu_z to decrease faster at the entrance, which contributes to the laminar flow towards a thermal fully developed region. This will have a negative influence on the enhancement of the heat transfer. Unlike the results presented by Rahimi and Mehryar [17], Fig. 4a, Fig. 5a and Fig. 6a present that Nu_z in the fully developed region is not always a constant value. Furthermore, in some cases Nu_z does not monotonically decrease from the inlet to the outlet, but demonstrates a local minimum near the entrance. Such minima are also reported in some numerical [12, 22, 31] and experimental [39] researches.

From the point view of *Nu*, in the entrance and ending regions, *Nu* varies significantly while in the fully developed region *Nu* varies less. Specifically, the average *Nu* deviations of all the 36 cases for the entrance region, for the fully development region and for the ending region are up to 21.516%, 1.829% and 4.415%, respectively. Here, the fully developed region is different from the "no wall" case, in which *Nu* remains constant. In the fully developed region discussed here, the thermal boundary layer converges at the central streamline though the temperature profile changes along the channel as shown in Fig. 15a. Besides, Fig. 15b indicates that the velocity profile does not change in the fully developed region even considering axial heat conduction.

Fig. 7 shows the Nusselt number deviation between the case with axial heat conduction and that without axial heat conduction as a function of *Pe*, k_{sf} and δ. Erro_*Nu* is calculated by Eq. (21). In Fig. 7, *Nu* decreases drastically with decreasing *Pe* at low *Pe* (*P*e≤500) and with increasing k_{sf} at low k_{sf} (k_{sf} ≤100). As axial heat conduction becomes dominant, *Pe* has more effects than k_{sf} and δ.

$$\text{Erro}\_\Delta Nu = \frac{Nu_{cp,wall} - Nu_{cp}}{Nu_{cp}} \times 100 \tag{21}$$

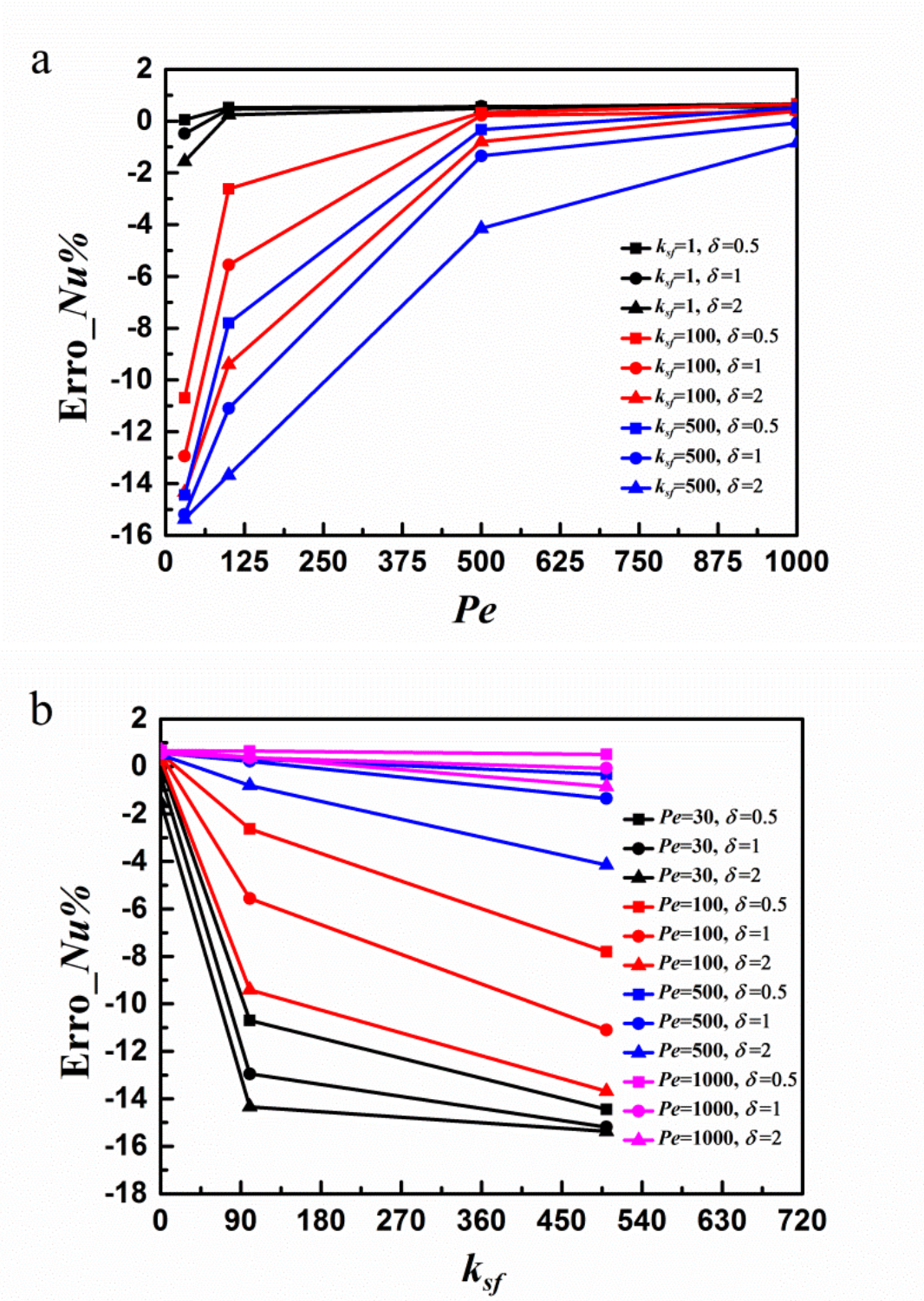
a
Erro_Nu%
Pe
0
125
250
375
500
625
750
875
1000
2
0
-2
-4
-6
-8
-10
-12
-14
-16
k_{sf}=1, δ=0.5
k_{sf}=1, δ=1
k_{sf}=1, δ=2
k_{sf}=100, δ=0.5
k_{sf}=100, δ=1
k_{sf}=100, δ=2
k_{sf}=500, δ=0.5
k_{sf}=500, δ=1
k_{sf}=500, δ=2
b
Erro_Nu%
k_{sf}
0
90
180
270
360
450
540
630
720
2
0
-2
-4
-6
-8
-10
-12
-14
-16
-18
Pe=30, δ=0.5
Pe=30, δ=1
Pe=30, δ=2
Pe=100, δ=0.5
Pe=100, δ=1
Pe=100, δ=2
Pe=500, δ=0.5
Pe=500, δ=1
Pe=500, δ=2
Pe=1000, δ=0.5
Pe=1000, δ=1
Pe=1000, δ=2

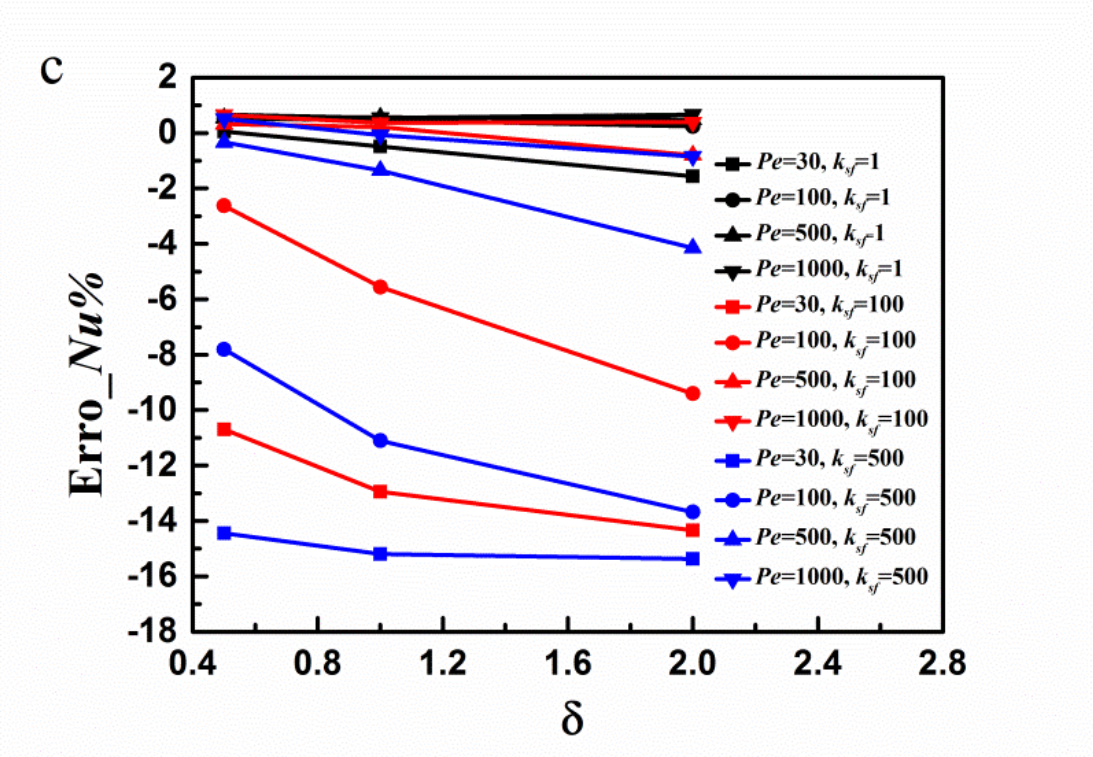

Fig.7. Effects of *Pe*, k_{sf} and δ on Erro_*Nu*.

3.2. Axial heat conduction with variable fluid properties

As mentioned earlier, in a real case the solid wall with strong axial heat conduction conducts a portion of heat from the downstream part back to the upstream part of the channel, leading to the redistribution of q^*, T_f^* and T_w^*, which finally contributes to the change of Nu_z. But most of the open published literatures take the fluid properties as constant when investigating the axial heat conduction. This section will further study the effects of the axial heat conduction allowing for variations in fluid properties.

When the flow is incompressible, property variations may occur due to the temperature or pressure dependent viscosity, thermal conductivity, specific heat capacity and other fluid properties. Among all the thermophysical properties, the present work selected dynamic viscosity and thermal conductivity as the most prominent and the most important fluid properties while other properties were kept

constant. Prandtl number ($Pr = \mu \cdot c_p / k$) is the characteristic number of a fluid. In the temperature ranges examined in this study, dynamic viscosity and thermal conductivity have the greatest change among the three kinds of thermophysical properties (μ , c_p , k). Fluid-property change rate for water, C10 and air from inlet to outlet is listed in Table 4. In addition, the influence of the pressure on the fluid properties was not considered. This assumption, though somehow unrealistic for certain fluid especially for gas, can clearly reveal the role played by the most prominent fluid properties from a research point of view. In this section, three different working fluids, i.e., water, C10 and air are selected since the behavior of both μ and k of the three fluids are different, which can represent the change of μ and k with temperature increase for most fluids. k used in the calculations of Nu_z by Eq. (13) was obtained according to the fluid bulk temperature. For water and C10, the numerical simulations were conducted within the temperature range of the liquid phase at atmospheric pressure. The air considered in this study was not ideal gas since its density remained constant. For the three kinds of fluids, the temperature-dependent μ and k were given by cubic polynomial fitting results of data from fluid property database REFPROP Version 9.0 developed by the National Institute of Standards and Technology [40] in the form of $k(T)/\mu(T) = a_0 + a_1 T + a_2 T^2 + a_3 T^3$, where a_0, a_1, a_2, a_3 were constant coefficients. The following work was conducted for the case with Pe=100, $k_{sf} = 100$ and $\delta = 1$ since variations in fluid properties were the focus of this section. While for water, the present work studied cases under different parameters related to the axial heat conduction.

Table 4 Fluid-property change rate for water, C10 and air (from inlet to outlet).

Fluid	Temperature range(℃)	Dynamic viscosity change rate (%)	Thermal conductivity change rate (%)
Water	50	-50.7	10.8
C10	120	-71.5	-22.0
Air	475	49.4	111.9

3.2.1. Effects of both separately and simultaneously variable $\mu(T)$ *and* $k(T)$ *on* Nu_z, q^*, T_f^* *and* T_w^*

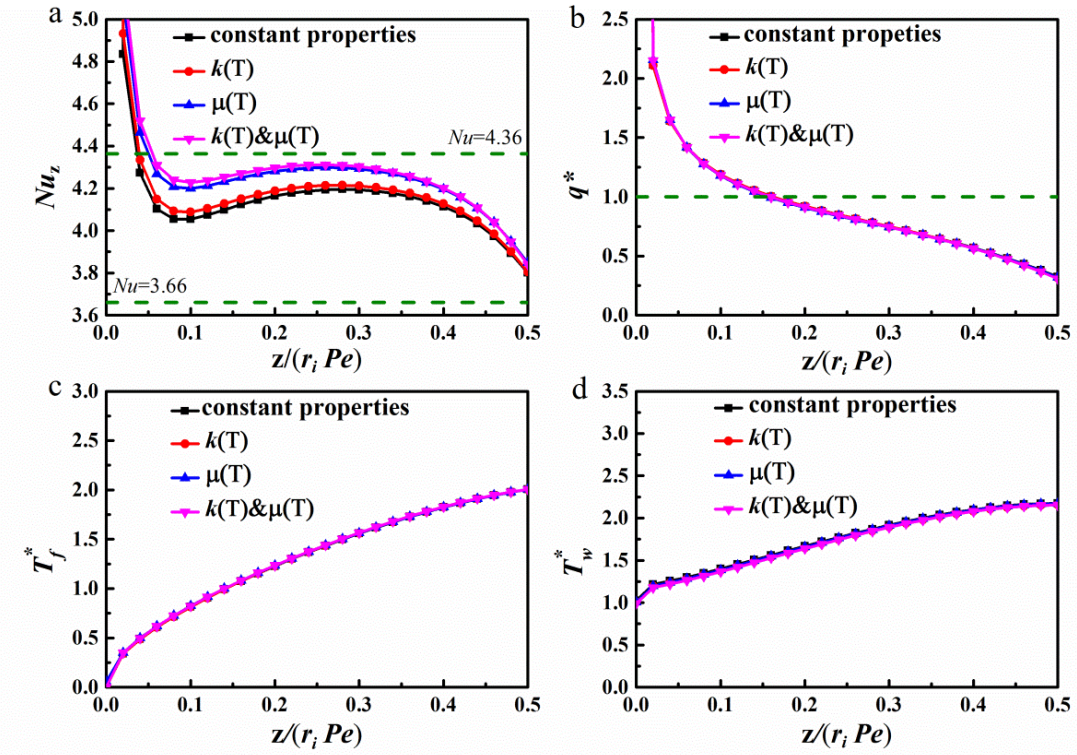

Fig. 8. Comparisons of the local values of relevant parameters between constant and variable properties of water. (a: Nu_z; b: q^*; c: T_f^*; d: T_w^*)

Comparisons of the local values of relevant parameters (Nu_z, q^*, T_f^* and T_w^*) between constant and variable properties for water are shown in Fig. 8. It is clear that Nu_z with variable $\mu(T)$ is much higher than that with constant properties. It is generally believed that a lower viscosity contributes to a higher velocity and a smaller boundary layer thickness, which is favorable for promoting convective heat transfer in the channel. Fig. 8 presents that Nu_z with variable $k(T)$ is a little higher than that

with constant properties. The thermal boundary layer thickness indicates the scale of temperature gradient across the flow and thus directly determines the local heat transfer performance. A higher thermal conductivity enhances the heat transfer performance. Therefore, the increase in thermal conductivity account for the higher Nu_z of water as temperature rises. Fig. 8 shows that Nu_z with both variable $\mu(T)$ and $k(T)$ is much higher than that with constant properties. Since water has a lower $\mu(T)$ level and a higher $k(T)$ level as temperature rises, the heat transfer in the heated tube is enhanced with variable $\mu(T)$ and $k(T)$ for water, both separately and simultaneously, within the temperature range considered here. It can also be seen from Fig. 8 that variations in fluid properties have little effects on q^*, T_f^* and T_w^* for water due to its small change rate of fluid properties.

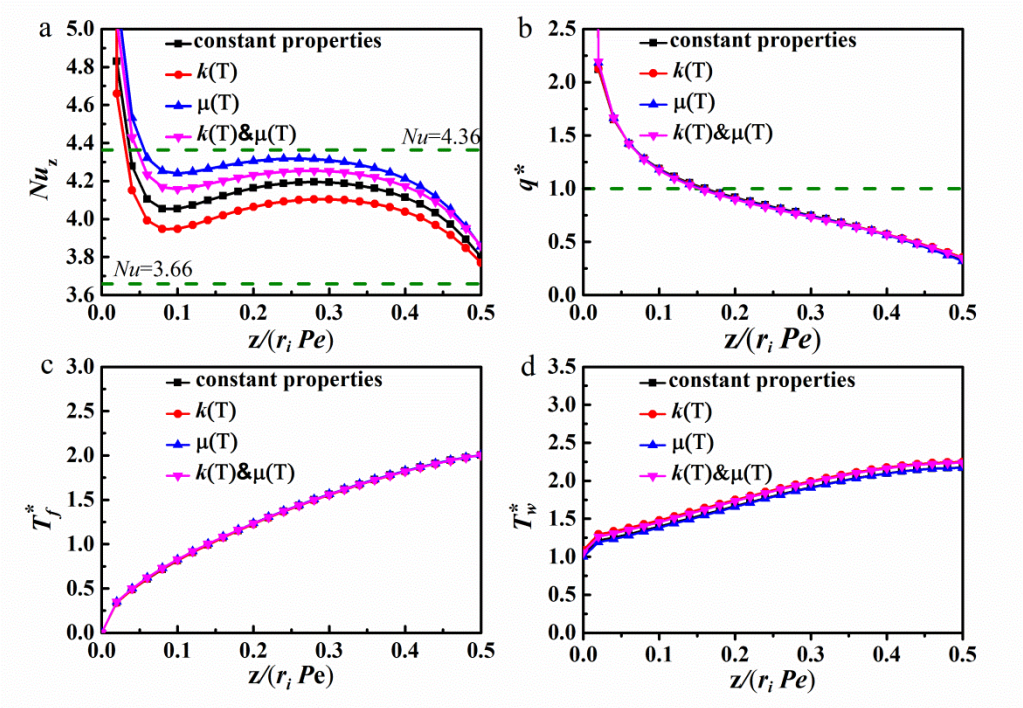

Fig. 9. Comparisons of the local values of relevant parameters between constant and variable properties of C10. (a: Nu_z; b: q^*; c: T_f^*; d: T_w^*)

In Fig. 9 the comparisons of the local values of relevant parameters (Nu_z, q^*, T_f^* and T_w^*) between constant and variable properties for C10 are shown. Since C10

has a lower $\mu(T)$ level as temperature rises, which contributes to promoting convective heat transfer in the channel, Nu_z of C10 with variable $\mu(T)$ is much higher than that with constant properties. Nu_z of C10 with variable $k(T)$ is lower than that with constant properties due to its lower $k(T)$ level as temperature rises. In addition, Nu_z of C10 with both variable $\mu(T)$ and $k(T)$ is higher than that with constant properties but lower than that with only variable $\mu(T)$. It appears that dynamic-viscosity variation dominates for C10. Fig. 9 also presents that variations in properties have little effects on q^* and T_f^* for C10 but cause T_w^* to be slightly higher than that of the constant properties.

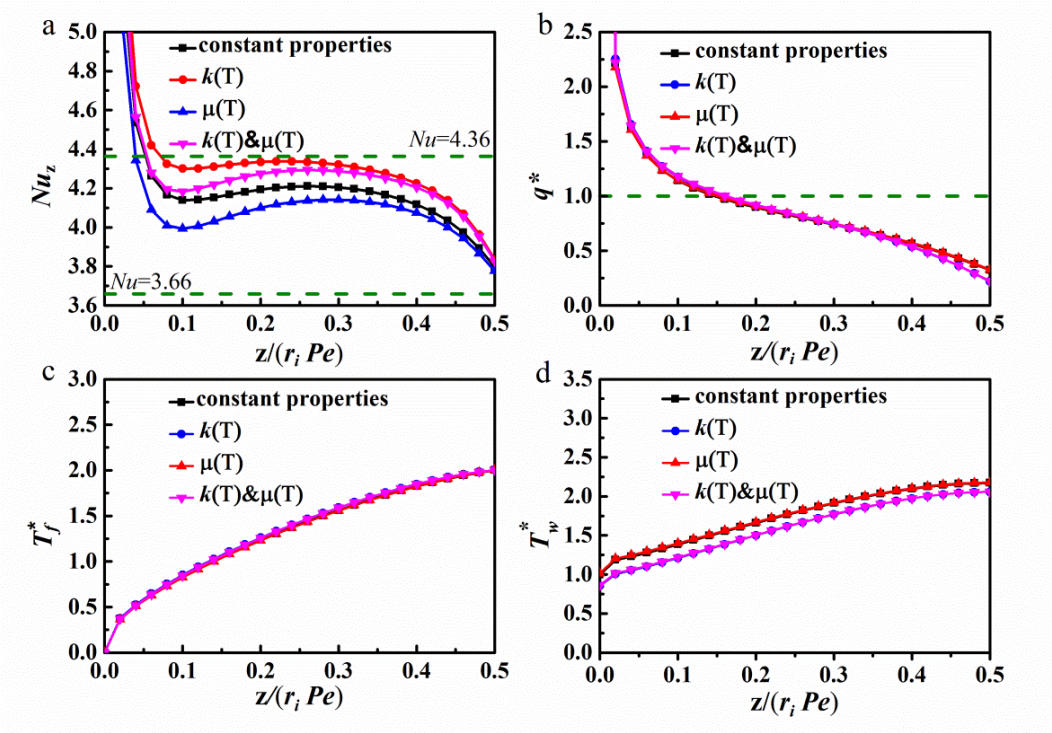

Fig. 10. Comparisons of the local values of relevant parameters between constant and variable properties of air. (a: Nu_z; b: q^*; c: T_f^*; d: T_w^*)

In Fig. 10 four figures are presented for the comparisons of the local values of relevant parameters (Nu_z, q^*, T_f^* and T_w^*) between constant and variable properties

for air. The higher $\mu(T)$ and $k(T)$ levels of air as temperature rises can explain the characteristics of Nu_z with constant and variable properties shown in Fig.10: (1) Nu_z with variable $\mu(T)$ is lower than that with constant properties; (2) Nu_z with variable $k(T)$ is higher than that with constant properties; (3) Nu_z with both variable $\mu(T)$ and $k(T)$ is higher than that with constant properties but lower than that with only variable $k(T)$; (4) Variations in properties have little effects on q^* and T_f^* for air, but causes T_w^* to be lower than that of the constant properties.

It is intuitive to predict a steep *Nu* jump near the front part of the tube due to the thin thermal boundary layer, regardless of variable- or constant-property flow, as hinted in Figs. 8-10. Though the variations of q^* and T_f^* are small, their combined effects together with the variations of T_w^* can cause Nu_z to deviate from that with constant properties. Variable-property effects cannot change the variation trend of the distribution of Nu_z, but variable dynamic viscosity and thermal conductivity affect more the upstream part of the channel for water and C10, while for air their effects are more notable at the downstream part of the channel. This so-called variable-property effects are evaluated by the *Nu* deviation, defined as follows:

$$\Delta Nu = \frac{Nu_{vp,wall} - Nu_{cp,wall}}{Nu_{cp,wall}} \times 100 \tag{22}$$

The maximum ΔNu of water, C10 and air are up to 7.33% at the entrance part, 4.45% at the entrance part, 2.20% at the ending part, respectively, and the average ΔNu of water, C10 and air are about 3.24%, 1.94%, 1.74%, respectively. It is also worth noting that, ΔNu for water and C10 due to variable $\mu(T)$ exceeds that due

to variable $k(T)$, while for air it is the opposite. This might be explained by the difference of fluid-property change rate considered in this work, as shown in Table 4. From water, C10 to air, the temperature range becomes larger and larger. These differences of dynamic-viscosity variation and thermal-conductivity variation are the reason why the dynamic-viscosity variation dominates for water and C10, but for air thermal-conductivity variation is more dominant. In any case, it seems that the effects of the simultaneous variations of $\mu(T)$ and $k(T)$ can be estimated by combining their separate effects qualitatively but not quantitatively.

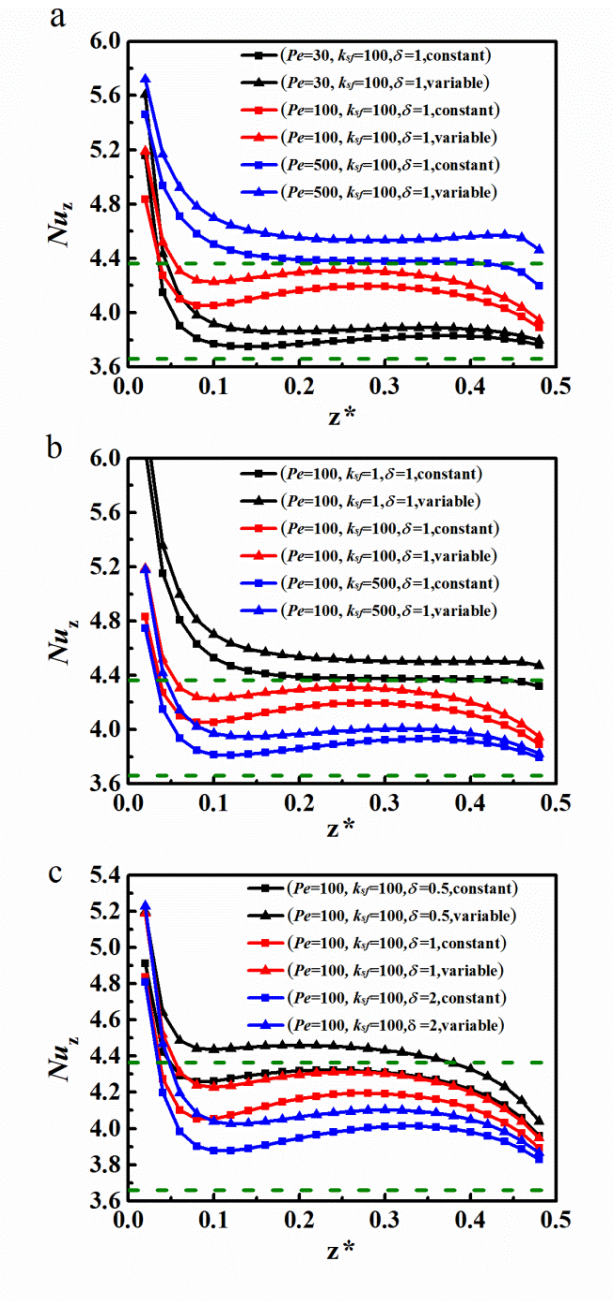

Fig. 11. Comparisons of Nu_z between constant and variable properties of water.

Fig. 11 illustrates the axial distribution of Nu_z with constant and variable properties with water as the working fluid in 14 cases. It is noted that as axial heat conduction becomes more dominant, variable-property effects become more notable at the entrance and weaken gradually as a result of axial heat conduction. Therefore, for water variable-property effects should be taken seriously at the entrance when axial heat conduction is dominant.

3.2.2. Effects of property variations on velocity and temperature profiles

In order to have a deep understanding of why the changes of relevant parameters (Nu_z, q^*, T_f^* and T_w^*) happen considering variable-property effects, this could be identified by analyzing the velocity and temperature profile characteristics. The velocity and temperature profiles of variable- and constant-property flows for water, C10 and air are depicted in Fig. 12-14, respectively, where black curves stand for constant-property flow while the other curves stand for variable-property flow. The axial velocity and temperature profiles in cross-section are drawn at two typical streamwise locations, i.e., z^*=0.025 at the entrance region and z^*=0.25 at the fully developed region.

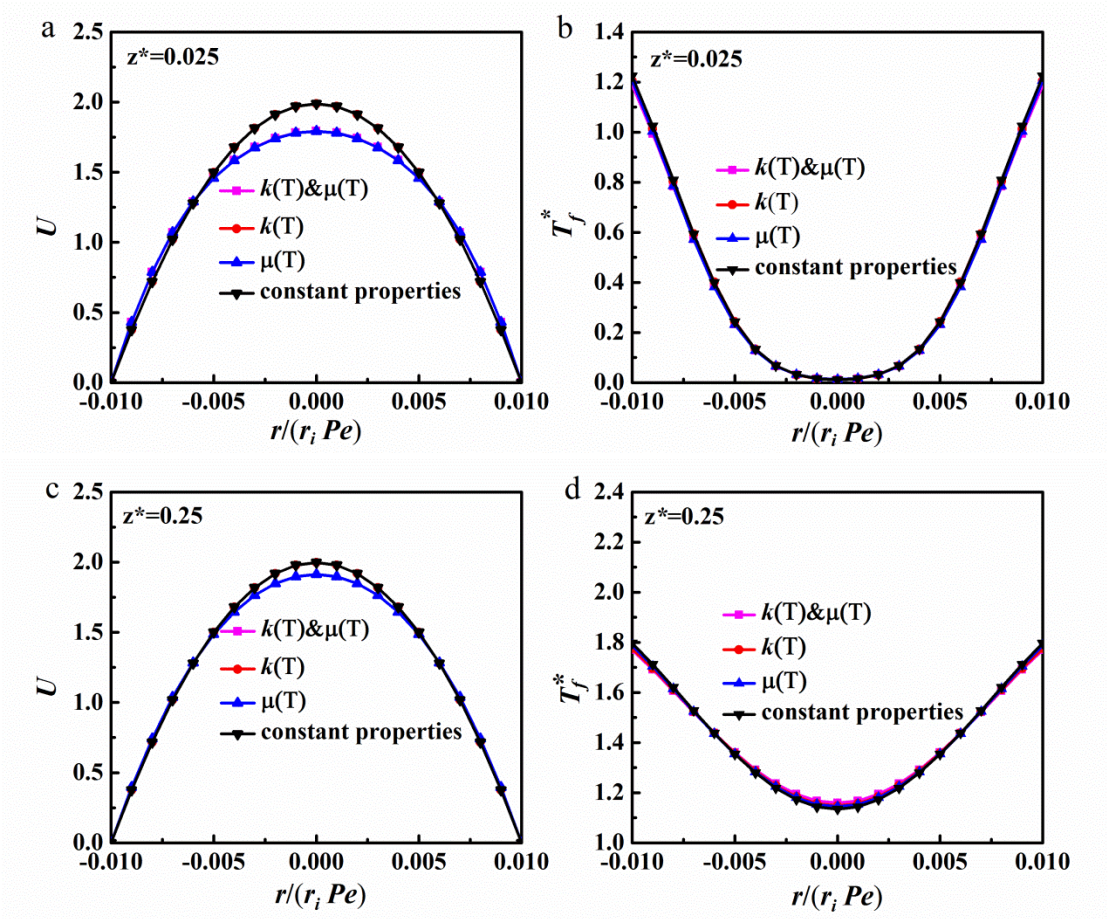

Fig. 12. Variations of axial velocity and temperature profiles in cross-section.
(water, a, b: z^*=0.025; c, d: z^*=0.25)

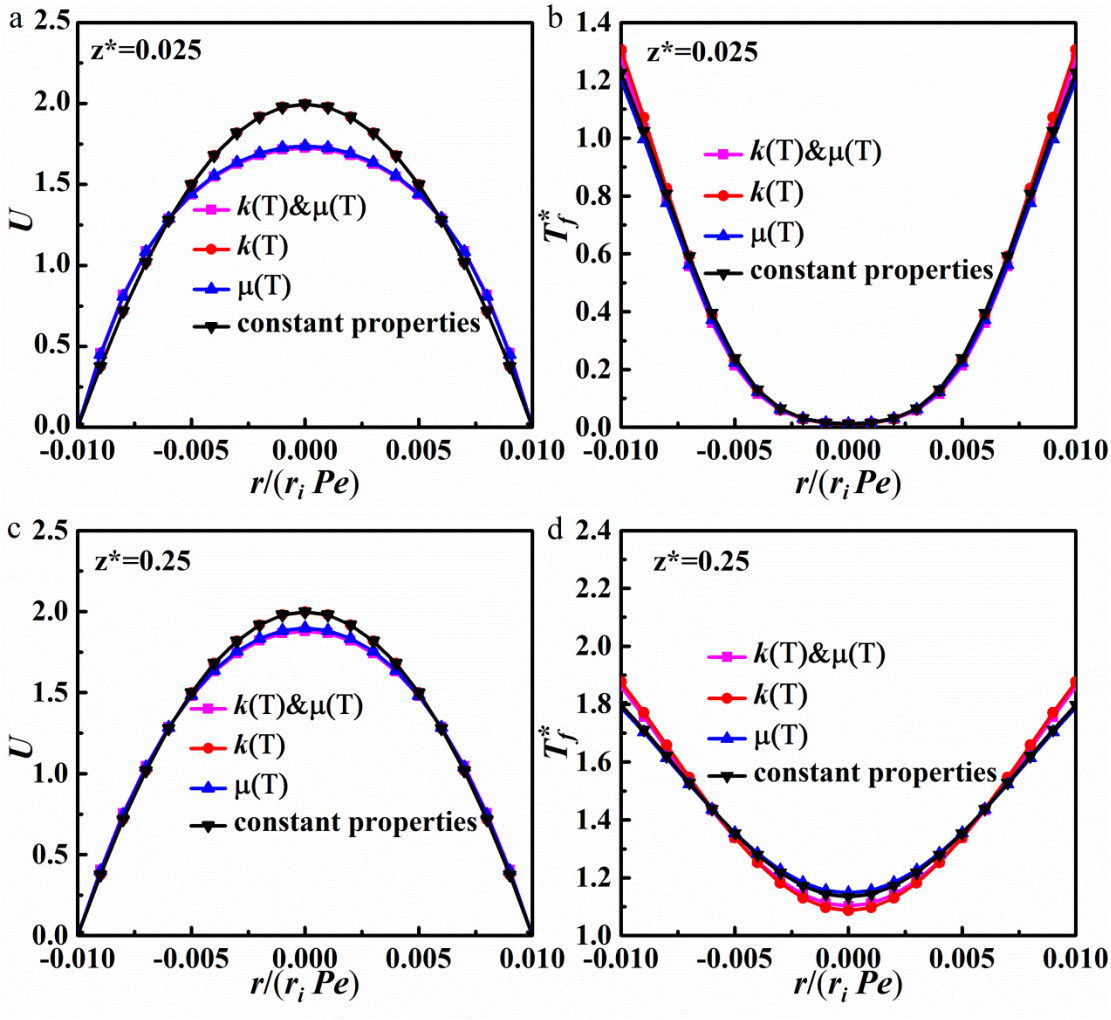

Fig. 13. Variations of axial velocity and temperature profiles in cross-section.
(C10, a, b: z^*=0.025; c, d: z^*=0.25)

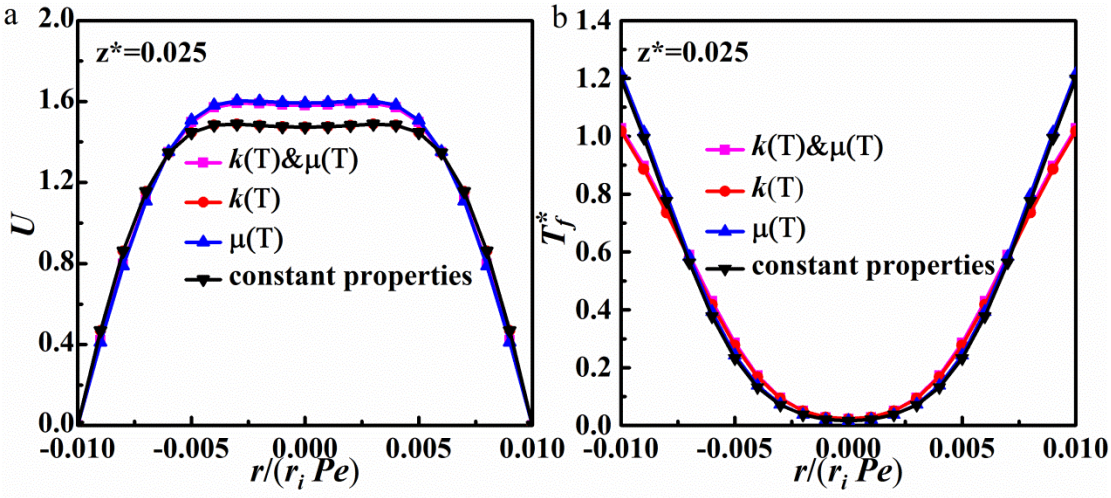

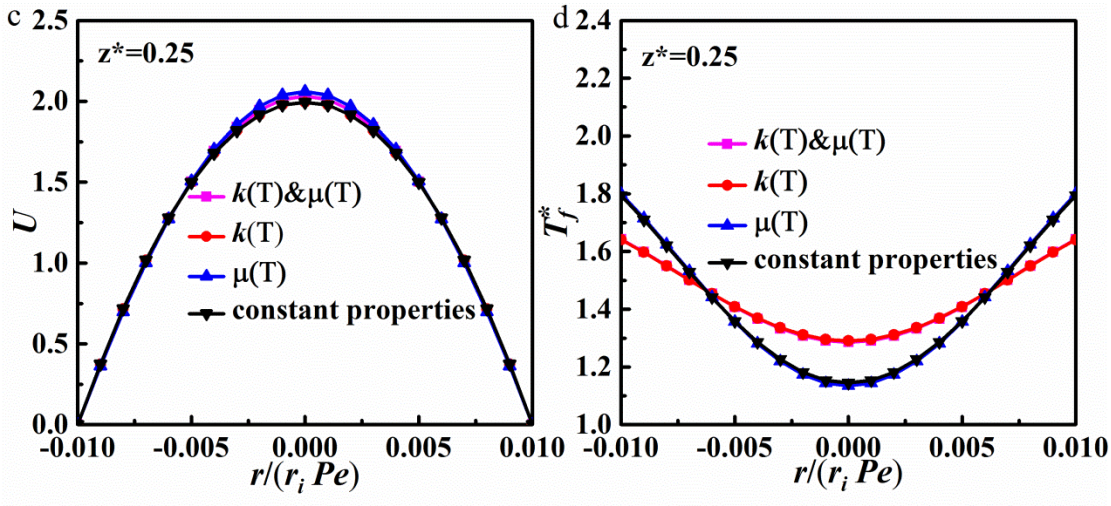

Fig.14. Variations of axial velocity and temperature profiles in cross-section.
(air, a, b: z^*=0.025; c, d: z^*=0.25)

Above figures show that the variable fluid properties have more notable effects on the velocity profile at the entrance region while more notable effects on temperature profile at the fully developed region. Since the air has the biggest changes of thermophysical properties compared with water and C10, variations in properties have the greatest effects on its velocity and temperature profiles. It is also noted that in Fig. 12a and c, Fig.13a and c, Fig.14a and c curves of constant k and variable $k(T)$ overlap very well with each other, which indicates that variable $k(T)$ has little effects on velocity profile. But variable $k(T)$ can affect the temperature profile as shown in Fig. 13b and d, Fig. 14b and d. Likewise, variations in $\mu(T)$ have greater effects on velocity profile than variations in $k(T)$. On the one hand, for water and C10, velocity profile with both variable $\mu(T)$ and $k(T)$ are flattened compared to that with constant properties while for air it is the opposite. Decrease in $\mu(T)$ due to higher temperature reduces axial velocity at the center and thus causes the flattening effect. This flattening effect leads to more mass flow rate near the wall, thereby enhancing heat convection. On the other hand, for water, the temperature profile of the variable properties changes a little. But for C10, the temperature profile

with variable $\mu(T)$ and $k(T)$ are steeper compared to that with constant properties while for air it is also the opposite. Decrease in $k(T)$ due to higher temperature reduces temperature gradient near the wall and thus weakens the heat convection. All these differences can be explained by the disparity of fluid-property changes as temperature rises.

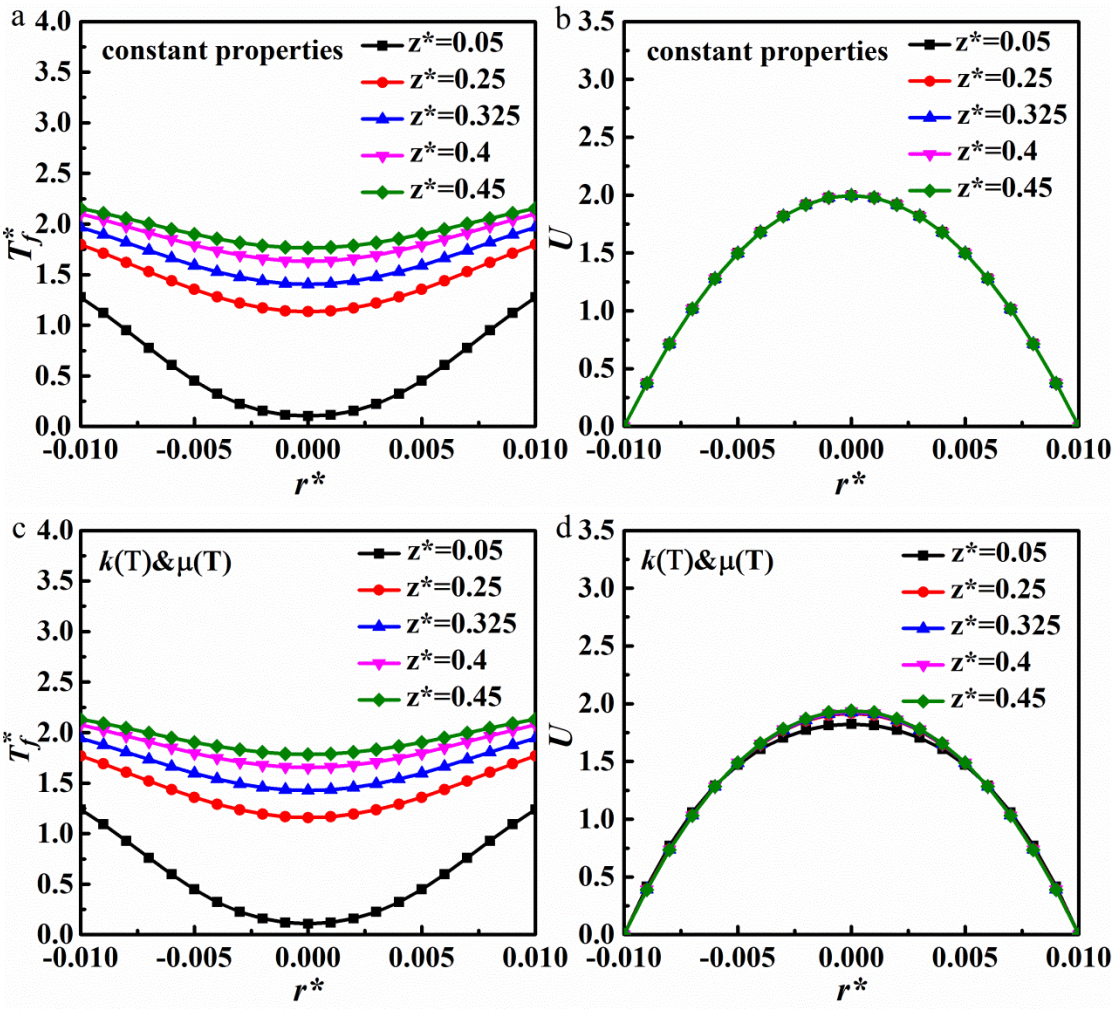

Fig. 15. Variations of axial velocity and temperature profiles in cross-section along the tube between constant and variable properties. (water, Pe=100, k_{sf}=100, Δ / d_i=1)

Fig. 15 plots the velocity and temperature profiles in cross-section along the tube with constant- and variable-property for water. For axial heat conduction with constant properties, the temperature profile changes along the channel while the velocity profile remains unchanged. As can be seen in Fig. 15c and d, there is a

change in the velocity and temperature profiles with varying $\mu(T)$ and $k(T)$ along the heated region. The velocity profile, however, changes slightly along the flow, not as much as the temperature profile. The velocity profile becomes steeper along the flow direction as a result of decreasing $\mu(T)$ of water. Likewise, as long as $k(T)$ varies with increasing fluid bulk temperature, the temperature profile changes unceasingly along the tube and never achieves an unchanged status.

4. Conclusions

A comprehensive numerical study of the effects of the axial heat conduction on tube laminar flow and heat transfer with uniform internal heat generation has been conducted considering temperature-dependent $\mu(T)$ and $k(T)$. The main conclusions can be described as follows:

(1) Axial heat conduction has generalized effects of reducing the local Nusselt number with respect to the "no wall" case. *Nu* is still changed even at the fully developed region, though the thermal boundary layer is converged at the central streamline. Axial heat conduction can make the entrance length decrease and sometimes cause a minimum in Nu_z distribution. Axial heat conduction becomes more dominant with increasing k_{sf} and δ, as well as with decreasing *Pe*. *Nu* decreases drastically with decreasing *Pe* when *Pe*$\leq$500 and with increasing k_{sf} when k_{sf} $\leq$100. As the axial heat conduction becomes more dominant, *Pe* has more effects than k_{sf} and δ.

(2) Variable-property effects alleviate the reduction in Nu_z due to the axial heat conduction, which enhances heat transfer characteristics of the channel. For the case of *Pe*=100, δ=1 and k_{sf}=100, the maximum ΔNu between constant and variable

properties are up to 7.33% at the entrance part for water in the temperature range of 50℃, and 4.45% at the entrance part for n-decane in the temperature range of 120℃, as well as 2.20% at the ending part for air in the temperature range of 475℃, respectively. In addition, the average ΔNu for water, n-decane and air are 3.24%, 1.94% and 1.74%, respectively. Namely, for water and C10 variable-property effects affect more the upstream part of the channel, while for air their effects are more notable at the downstream part of the channel.

(3) For the axial heat conduction with constant properties, the temperature profile changes along the channel while the velocity profile remains unchanged. On the other hand, for the axial heat conduction with variable properties, both temperature and velocity profiles keep changing along the channel and the change of temperature profile is larger. Besides, variable properties have more obvious effects on the velocity profile at the upstream part while more obvious effects on the temperature profile at the downstream part.

References

[1] H. Herwig, O. Hausner, Critical view on “new results in micro-fluid mechanics”: an example. International Journal of Heat and Mass Transfer, 2003, 46(5):935-937.

[2] G. Hetsroni, A. Mosyak, E. Pogrebnyak, L.P. Yarin, Heat transfer in micro-channels: Comparison of experiments with theory and numerical results. International Journal of Heat and Mass Transfer, 2005, 48(25):5580-5601.

[3] M. Faghri, E. M.Sparrow, Simultaneous wall and fluid axial conduction in laminar pipe-flow heat transfer. Journal of Heat Transfer, 1980, 102(1):58-63.

[4] C. J. Kroeker, H. M. Soliman, S. J. Ormiston, Three-dimensional thermal analysis of heat sinks with circular cooling micro-channels. International Journal of Heat and

Mass Transfer, 2004, 47(22):4733-4744.

[5] J. Li, G. P. Peterson, P. Cheng, Three-dimensional analysis of heat transfer in a micro-heat sink with single phase flow. International Journal of Heat and Mass Transfer, 2004, 47(19-20):4215-4231.

[6] E. K. Zariffeh, H. M. Soliman, A. C. Trupp, Combined effects of wall and fluid axial conduction on laminar heat transfer in circular tubes. Begel House Inc, 1982:131-136.

[7] S. Bilir, Laminar flow heat transfer in pipes including two-dimensional wall and fluid axial conduction. International Journal of Heat and Mass Transfer, 1995, 38(9):1619-1625.

[8] A. E. Quintero, M. Vera, Laminar counterflow parallel-plate heat exchangers: An exact solution including axial and transverse wall conduction effects. International Journal of Heat and Mass Transfer, 2017, 104:1229-1245.

[9] E. J. Davis, W. N. Gill, The effects of axial conduction in the wall on heat transfer with laminar flow. International Journal of Heat and Mass Transfer, 1970, 13(3):459-470.

[10] A. O. Adelaja, J. Dirker, J. P. Meyer, Effects of the thick walled pipes with convective boundaries on laminar flow heat transfer. Applied Energy, 2014, 130(5):838-845.

[11] M. Axtmann, M. Heier, W. Hilali, B. Weigand, Axial heat conduction effects in the thermal entrance region for flows in concentric annular ducts: Correlations for the local bulk-temperature and the Nusselt number at the outer wall. International Journal of Heat and Mass Transfer, 2016, 103:974-983.

[12] C. Nonino, S. Savino, S. D. Giudice, L. Mansutti, Conjugate forced convection and heat conduction in circular microchannels. International Journal of Heat and Fluid

Flow, 2009, 30(5):823-830.

[13] S. X. Zhang, Y. L. He, G. Lauriat, W. Q. Tao, Numerical studies of simultaneously developing laminar flow and heat transfer in microtubes with thick wall and constant outside wall temperature. International Journal of Heat and Mass Transfer, 2010, 53(19):3977–3989.

[14] K. C. Toh, X. Y. Chen, J. C. Chai, Numerical computation of fluid flow and heat transfer in microchannels. International Journal of Advanced Manufacturing Technology, 2005, 26(5-6):537-543.

[15] G. Gamrat, M. Favre-Marinet, D. Asendrych, Conduction and entrance effects on laminar liquid flow and heat transfer in rectangular microchannels. International Journal of Heat and Mass Transfer, 2005, 48(14):2943-2954.

[16] G. Maranzana, I. Perry, D. Maillet, Mini- and micro-channels: influence of axial conduction in the walls. International Journal of Heat and Mass Transfer, 2004, 47(17):3993-4004.

[17] M. Rahimi, R. Mehryar, Numerical study of axial heat conduction effects on the local Nusselt number at the entrance and ending regions of a circular microchannel. International Journal of Thermal Sciences, 2012, 59(2):87-94.

[18] M. Lin, Q. W. Wang, Z. Guo, Investigation on evaluation criteria of axial wall heat conduction under two classical thermal boundary conditions. Applied Energy, 2016, 162:1662-1669.

[19] R. Kumar, S. P. Mahulikar, Effect of temperature-dependent viscosity variation on fully developed laminar microconvective flow. International Journal of Thermal Sciences, 2015, 98:179-191.

[20] C. J. Ho, C. Y. Chang, C. Y. Cheng, S. J. Cheng, Y. W. Guo, S. T. Hsu, W. M. Yan, Laminar forced convection effectiveness of Al_2O_3–water nanofluid flow in a circular

tube at various operation temperatures: Effects of temperature-dependent properties]. International Journal of Heat and Mass Transfer, 2016, 100:464-481.

[21] I. Ghosh, S. K. Sarangi, P. K. Das, Simulation algorithm for multistream plate fin heat exchangers including axial conduction, heat leakage, and variable fluid property. Journal of Heat Transfer, 2007, 129(7):884-893.

[22] D. Lelea, The conjugate heat transfer of the partially heated microchannels. Heat and Mass Transfer, 2007, 44(1):33-41.

[23] C. Nonino, S. D. Giudice, S. Savino, Temperature dependent viscosity effects on laminar forced convection in the entrance region of straight ducts. International Journal of Heat and Mass Transfer, 2006, 49(23-24):4469-4481.

[24] S. D. Giudice, C. Nonino, S. Savino, Effects of viscous dissipation and temperature dependent viscosity in thermally and simultaneously developing laminar flows in microchannels. International Journal of Heat and Fluid Flow, 2007, 28(1):15-27.

[25] S. P. Mahulikar, H. Herwig, Theoretical investigation of scaling effects from macro-to-microscale convection due to variations in incompressible fluid properties. Applied Physics Letters, 2005, 86(1):014105 - 014105-3.

[26] H. Herwig, S. P. Mahulikar, Variable property effects in single-phase incompressible flows through microchannels. International Journal of Thermal Sciences, 2006, 45(10):977-981.

[27] S. P. Mahulikar, H. Herwig, Physical effects in laminar microconvection due to variations in incompressible fluid properties. Physics of Fluids, 2006, 18(7):073601-073601-12.

[28] S. P. Mahulikar, H. Herwig, Physical effects in pure continuum-based laminar micro-convection due to variation of gas properties. Journal of Physics D: Applied

Physics, 2006, 39(18):4116-4123.

[29] H. P. Gulhane, S. P. Mahulikar, Variations in gas properties in laminar micro-convection with entrance effect. International Journal of Heat and Mass Transfer, 2009, 52(7-8):1980-1990.

[30] H. P. Gulhane, S. P. Mahulikar, Numerical study of compressible convective heat transfer with variations in all fluid properties. International Journal of Thermal Sciences, 2010, 49(5):786-796.

[31] A. Ramiar, A. A. Ranjbar, S. F. Hosseinizadeh, Effect of axial conduction and variable properties on two-dimensional conjugate heat transfer of Al2O3-EG/water mixture nanofluid in microchannel. Journal of Applied Fluid Mechanics, 2012, 5(3):79-87.

[32] G. L. Morini, Scaling effects for liquid flows in microchannels. Heat Transfer Engineering, 2006, 27(27):64-73.

[33] Z. G. Li, X. L. Huai, Y. J. Tao, H. Z. Chen, Effects of thermal property variations on the liquid flow and heat transfer in microchannel heat sinks. Applied Thermal Engineering, 2007,27(17-18):2803-2814.

[34] L. C. Burmerister, Convective Heat Transfer, John Weily & Sons, 1983.

[35] ANSYS CFX-Solver Theory Guide. ANSYS Inc., 2013.

[36] S. V. Patankar, D. B. Spalding, A calculation procedure for heat, mass and momentum transfer in three-dimensional parabolic flows. International Journal of Heat and Mass Transfer, 1972, 15(10):1787-1806.

[37] W. M. Kays, M. E. Crawford, B. Weigand, Convective Heat and Mass Transfer, fourth ed., McGraw-Hill, New York,1980.

[38] R. K. Shah, A. L. London, Laminar Flow Forced Convection in Ducts, Academic Press, New York, 1978.

[39] D. Lelea, S. NishioS, K. Takano, The experimental research on microtube heat transfer and fluid flow of distilled water. International Journal of Heat and Mass Transfer, 2004, 47(12):2817-2830.

[40] Lemmon E, Huber M, McLinden M. NIST Standard Reference Database 23, NIST Reference Fluid Thermodynamic and Transport Properties-REFPROP, Version 9.0. Standard Reference Data Program, National Institute of Standards and Technology: Gaithersburg, MD, 2010.